CCD's For X-ray Astronomy

George Chartas, Penn State University

3rd INTERNATIONAL X-RAY ASTRONOMY SCHOOL

OVERVIEW

- Charge-Coupled Devices, Basic Principles
- CCD's onboard *Chandra* and *XMM-Newton*
- CCD Performance : Energy Resolution, Quantum Efficiency
- Pileup, Charge Transfer Inefficiency, Contamination, Background, Subpixel Resolution
- Operating Modes, Event Processing
- CCD's In Future X-ray Astronomy Missions

This presentation follows a similar lecture made by M. Bautz (MIT) during the 2nd International X-ray School

3rd INTERNATIONAL X-RAY ASTRONOMY SCHOOL

Charge-Coupled Devices; Basic Principles

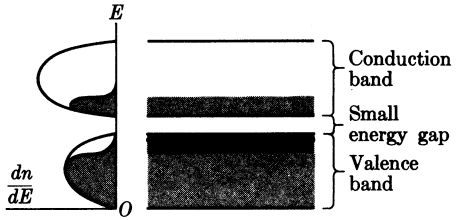

Fig. 6–39. Energy bands and electron distribution in a semiconductor.

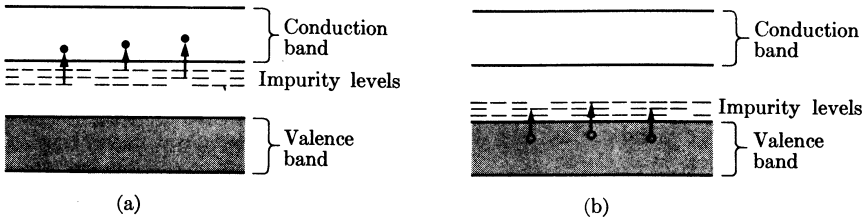

Fig. 6–40. Impurities in a semiconductor: (a) donors, or n-type, (b) acceptors, or p-type.

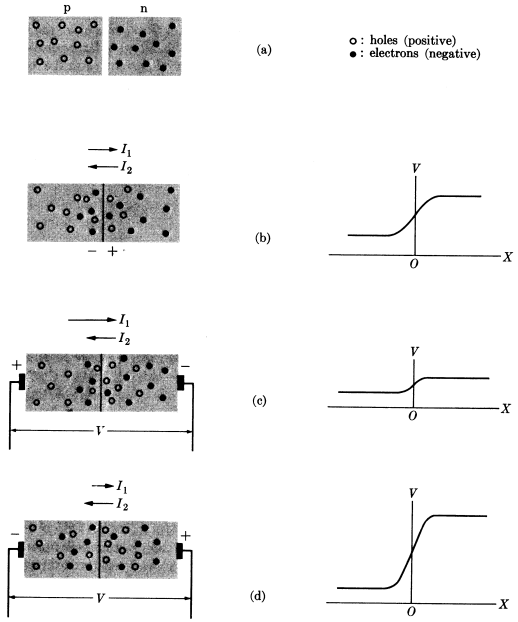

Fig. 6–41. The p-n junction.

- Valence bands, conduction bands and energy gaps in solids
- n and p-type semiconductors
- A p-n junction contains a narrow region on either side of the junction in which the majority charge carriers are "depleted".
- Electron-hole pairs created by photons absorbed in the depletion layer will be swept away by the potential difference across the junction before they recombine.

Charge-Coupled Devices; Basic Principles

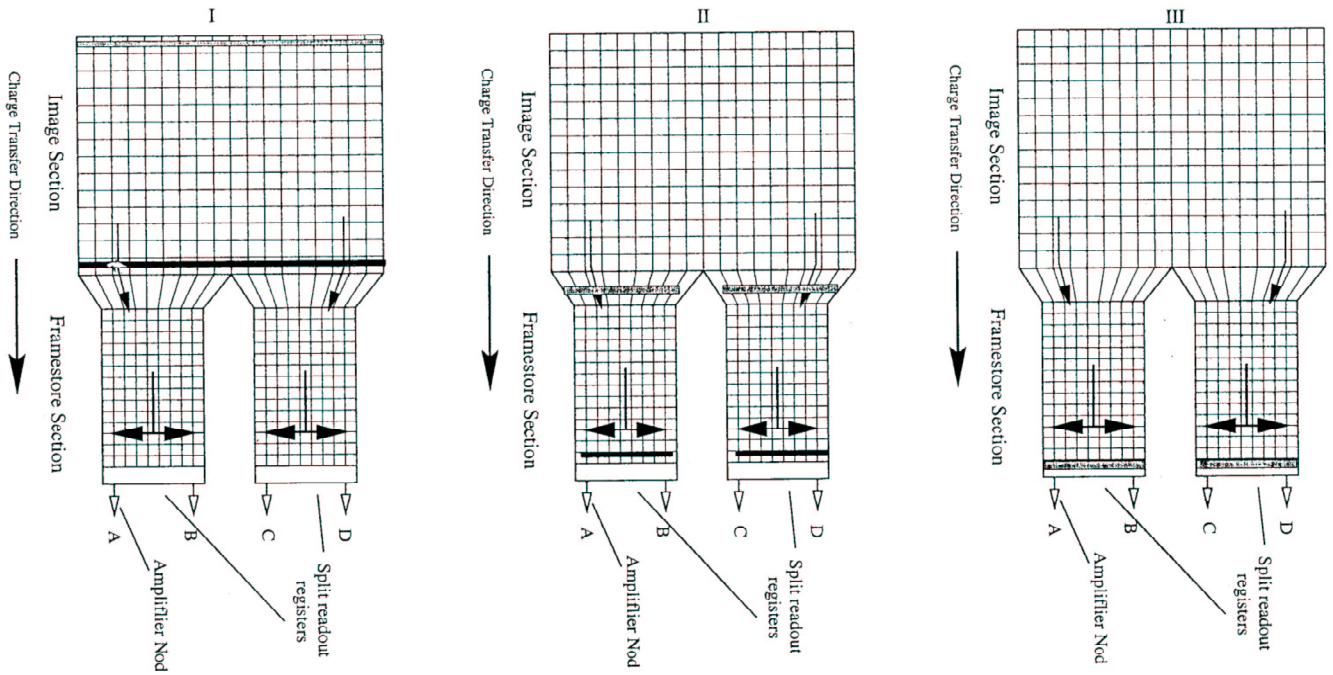

- A CCD is a grid of pixels each one of which can absorb photons and confine the resulting photoelectrons. To create an image device one needs the clock-away and collect the charge stored in individual pixels.

- Shown above is the layout of the ACIS CCDs. These devices were developed at MIT Lincoln Laboratory on high-purity p-type wafers of silicon. Each CCD is a 1024x1026-pixel (24 x 24 μm) frame-store imager which is divided into four sectors. The framestore is split, and the framestore pixels are 21 x 13.5 μm in size slightly smaller than those in the imaging area. This arrangement allows for four independent output amplifiers (nodes), and facilitates 3-side abutment of the detectors.

Charge-Coupled Devices; Basic Principles

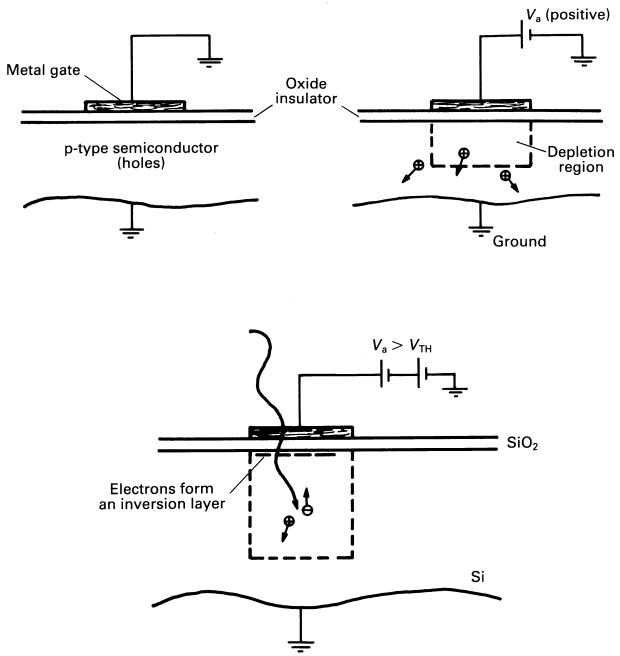

Fig. 6.7. A single metal-oxide-semiconductor (MOS) storage well, the basic element in a CCD.

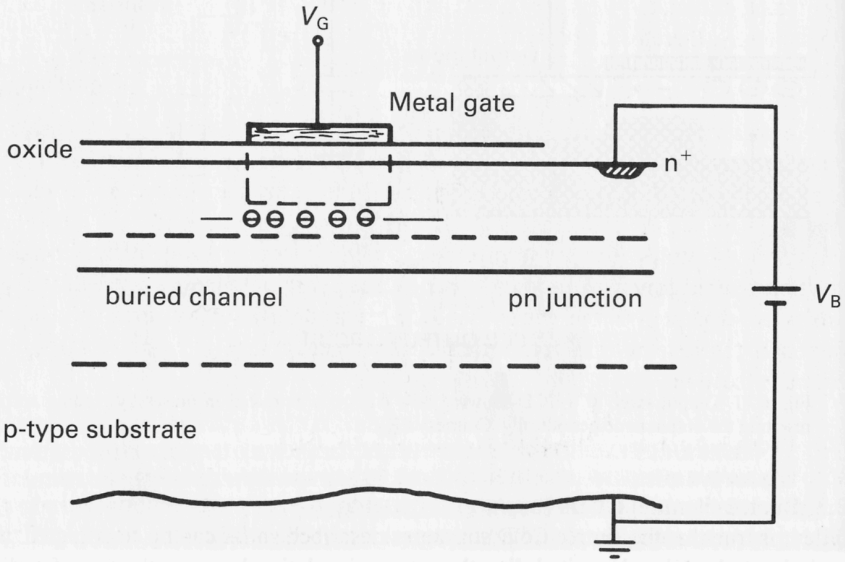

Fig. 6.12. (a) A single storage site in the buried-channel type of CCD. As the gate voltage increases the depleted zones finally meet.

MOS (Metal - Oxide-Semiconductor) One way of confining charge in a CCD pixel is achieved by depositing metal electrodes (gates) to a p-type semiconductor together with a thin layer of an oxide insulator. By applying a positive voltage on the gates, holes are swept out of a small region just below the insulator (depletion region). An X-ray photon absorbed in the depletion region will create electron-hole pairs. The electric field in the depletion region will prevent them from recombining and the electrons will be collected just below the oxide layer.

Buried-Channel CCDs To reduce charge trapping that occurs during the storage and transfer of charge located near the oxide insulator, an additional layer of n-type semiconductor is placed onto the existing p-type substrate to separate it from the oxide insulator. Essentially a p-n junction is created with a depletion layer located beneath the insulating layer (buried-channel CCD).

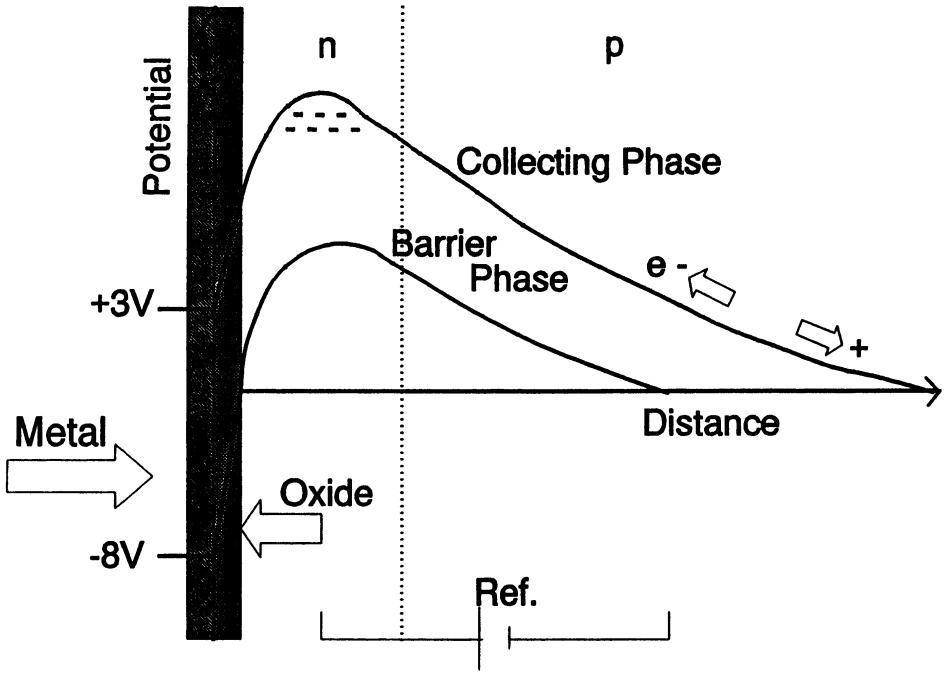

Fig. 6.12. (b) The collection layer lies well below the surface at the overlap between the gate depletion and the depletion of the pn junction. Courtesy Jim Janesick.

Charge-Coupled Devices; Basic Principles

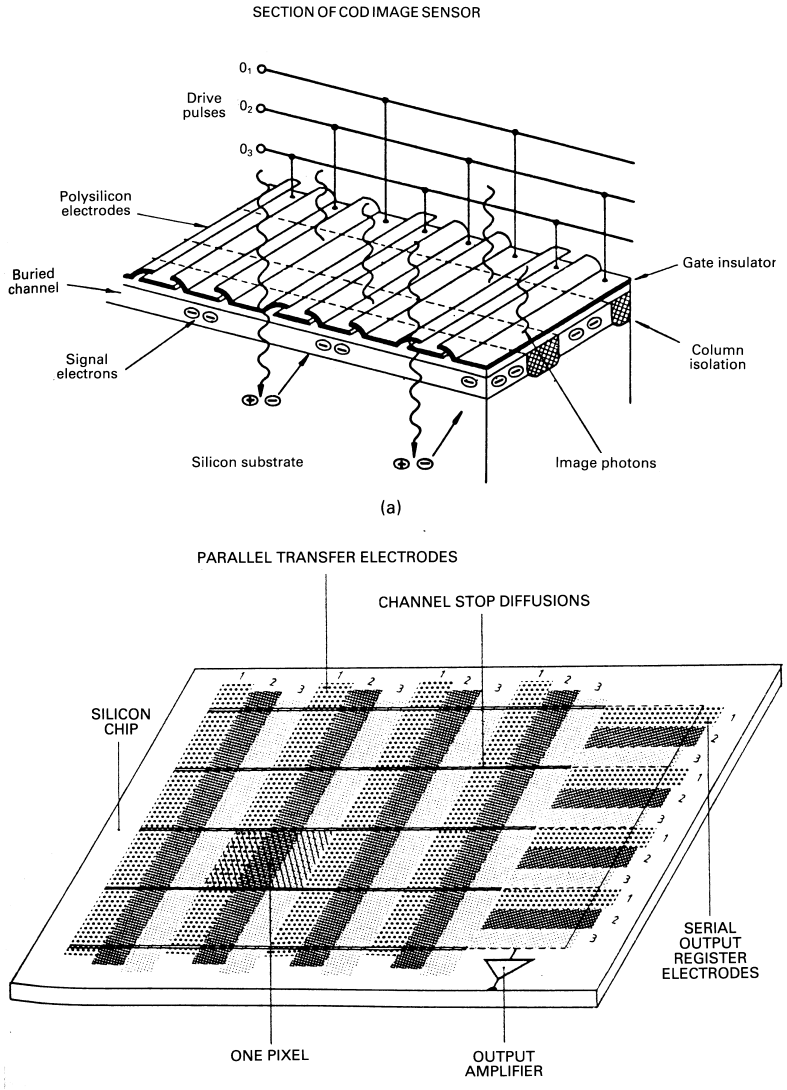

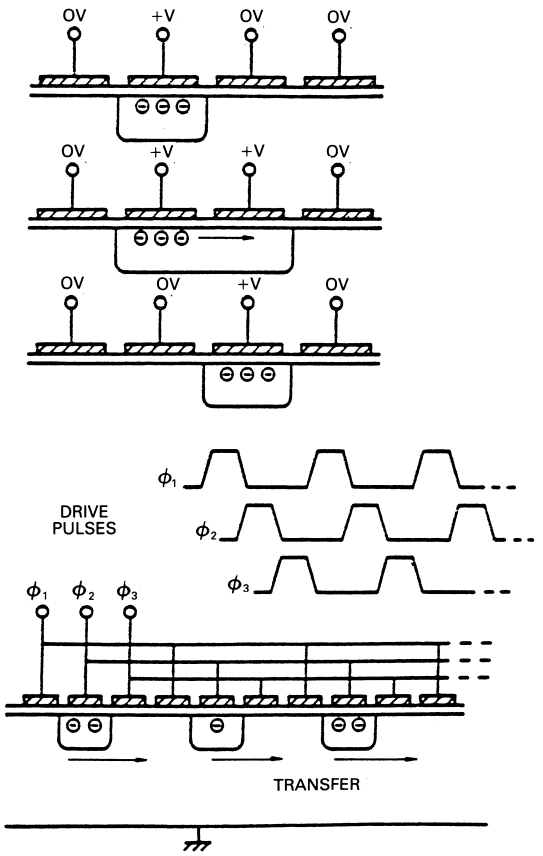

Fig. 6.9. Charge-coupling in a three-phase CCD and the associated timing waveform or clock pattern. In practice the degree of overlap between one electrode and the next depends on the CCD design.

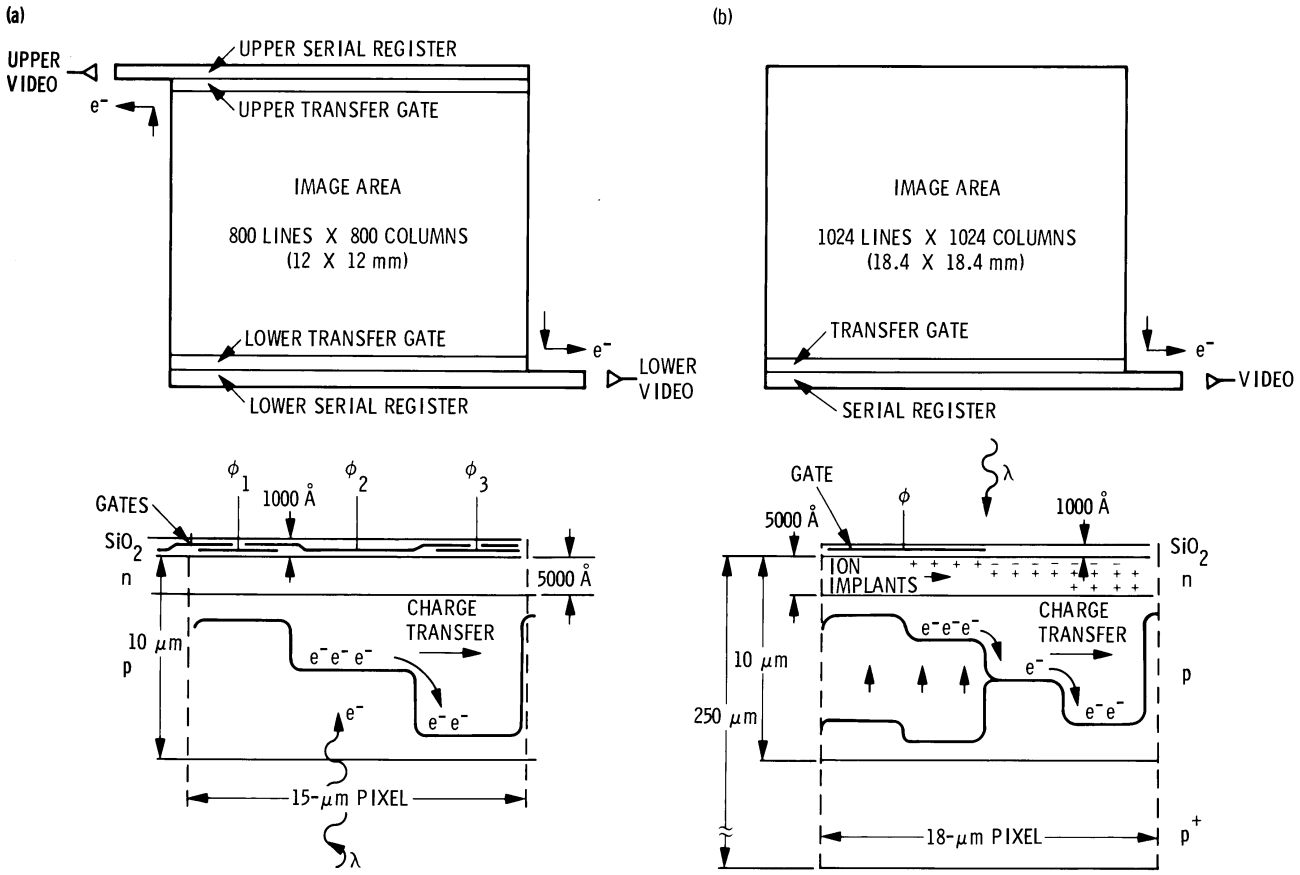

Fig. 6.14. Detailed comparison of the structure and dimensions of two CCDs from Texas Instruments. (a) A thinned and backside-illuminated three-phase CCD, and (b) the thick, front-illuminated virtual-phase device. Courtesy Jim Janesick.

CCD's Onboard *XMM-Newton*

The MOS EEV CCD22 is a three-phase frame transfer device on high resistivity epitaxial silicon with an open-electrode structure; it has a useful quantum efficiency in the energy range 0.2 to 10 keV. The low energy response of the conventional front illuminated CCD is poor below ~700 eV because of absorption in the electrode structure. For EPIC MOS, one of the three electrodes has been enlarged to occupy a greater fraction of each pixel, and holes have been etched through this enlarged electrode to the gate oxide. This gives an "open" fraction of the total pixel area of 40%; this region has a high transmission for very soft X-rays that would have otherwise be absorbed in the electrodes. In the etched areas, the surface potential is pinned to the substrate potential by means of "pinning implant". High energy efficiency is defined by the resistivity of the epitaxial silicon (around 400 Ohm-cm). The epitaxial layer is 80 microns thick (p-type). The actual mean depletion of the flight CCDs is between 35 to 40 microns: the open phase region is not fully depleted. Image and caption taken from http://xmm.vilspa.esa.es/external/xmm_user_support/documentation/technical/EPIC

CCD's Onboard *XMM-Newton*

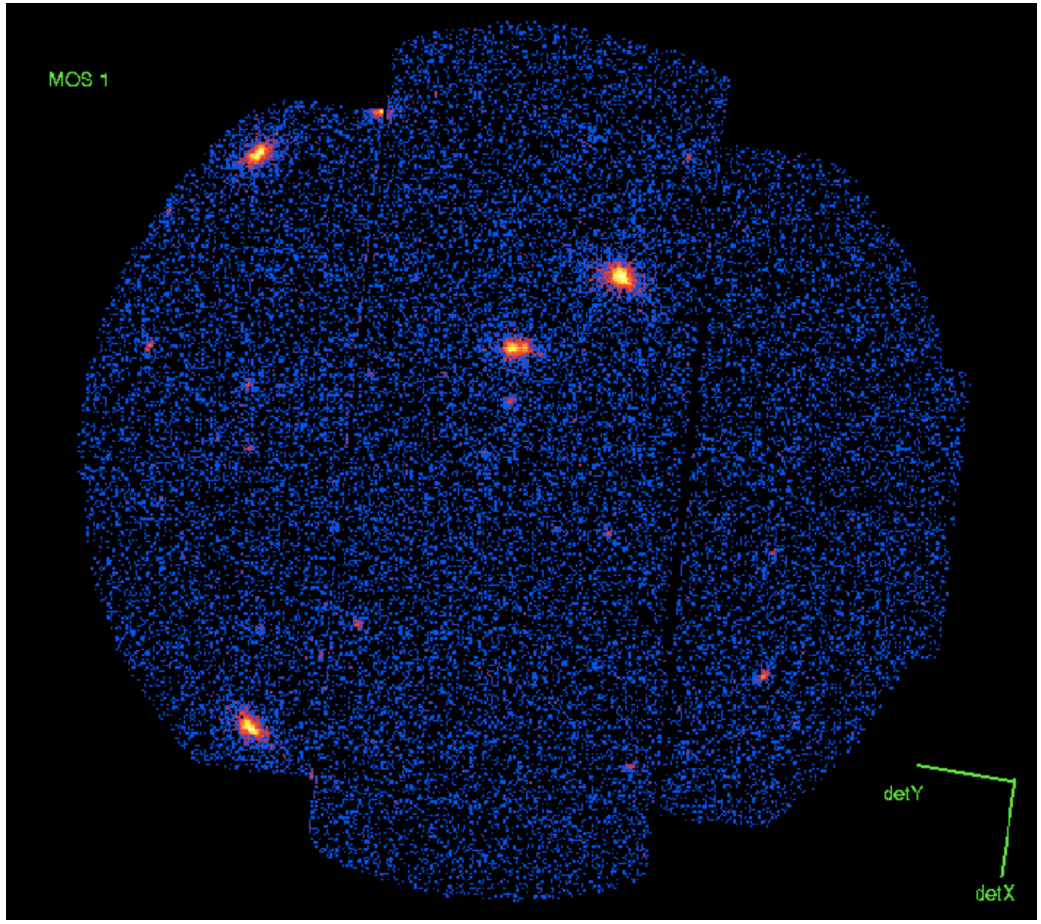

The field of view of the EPIC MOS 1 cameras: The camera detector co-ordinate frames are noted. 7 CCD's each 10.9 x 10.9 arcmin

CCD's Onboard *XMM-Newton*

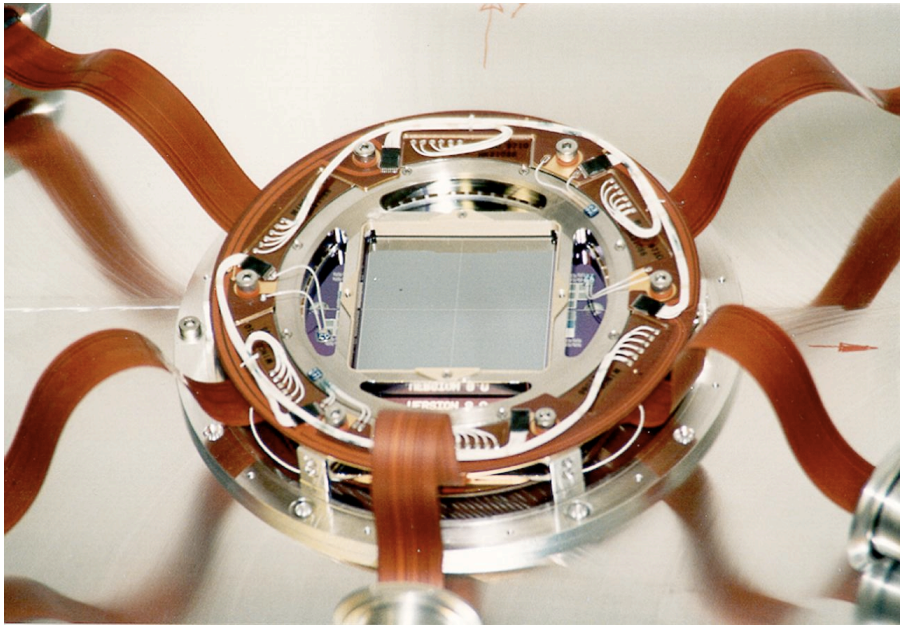

The PN-CCDs are back-illuminated. In the event of an X-ray interaction with the silicon atoms, electrons and holes are generated in numbers proportional to the energy of the incident photon. The average energy required to form an electron-hole pair is 3.7 eV at -90° C. The strong electric fields in the pn-CCD detector separate the electrons and holes before they recombine. Signal charges (in our case electrons), are drifted to the potential minimum and stored under the transfer registers. The positively charged holes move to the negatively biased back side, where they are 'absorbed'. The electrons, captured in the potential wells 10 microns below the surface can be transferred towards the readout nodes upon command, conserving the local charge distribution patterns from the ionization process. Each CCD line is terminated by a readout amplifier. The picture shows the twelve chips mounted and the connections to the integrated preamplifiers.
Image and caption from http://xmm.vilspa.esa.es/external/xmm_user_support/documentation/technical/EPIC/index.shtml#2.2

CCD's Onboard *XMM-Newton*

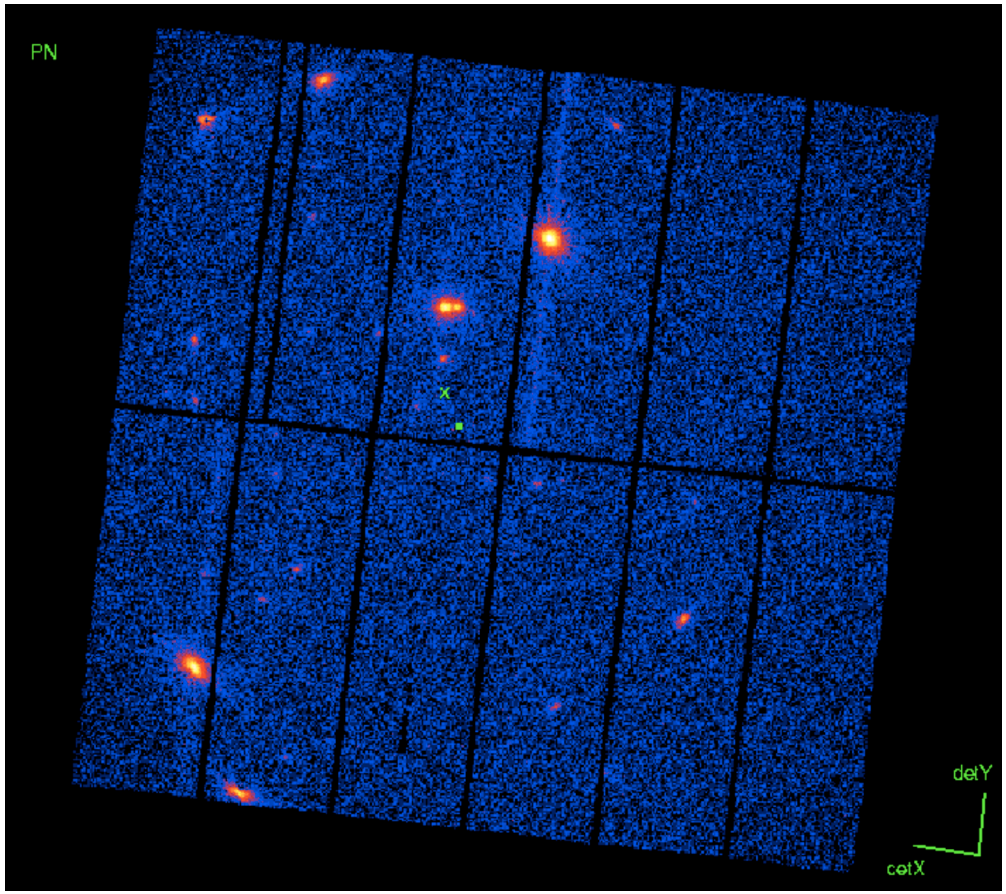

The field of view of the EPIC pn camera; The EPIC prime boresight is marked with a small box. 12 CCD's each 13.6 x 4.4 arcmin.

CCD's Onboard *Chandra*

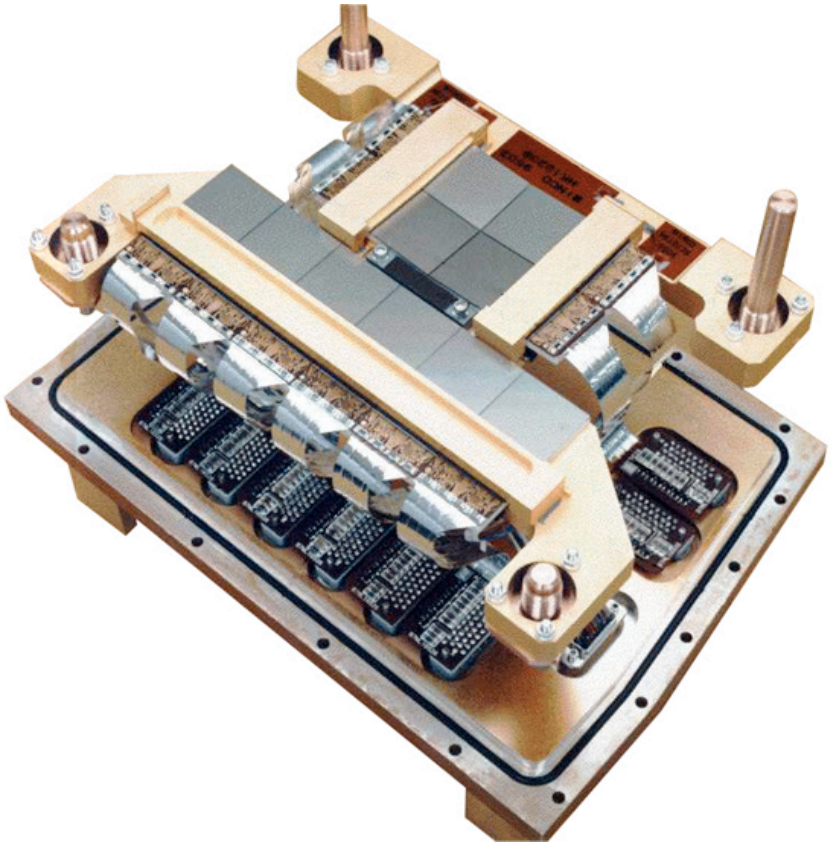

The Advanced CCD Imaging Spectrometer (ACIS) contains 10 planar, 1024 x 1024 pixel CCDs ; four arranged in a 2x2 array (ACIS-I) used for imaging, and six arranged in a 1x6 array (ACIS-S) used either for imaging or as a grating readout. Two CCDs are back-illuminated (BI) and eight are front-illuminated (FI).

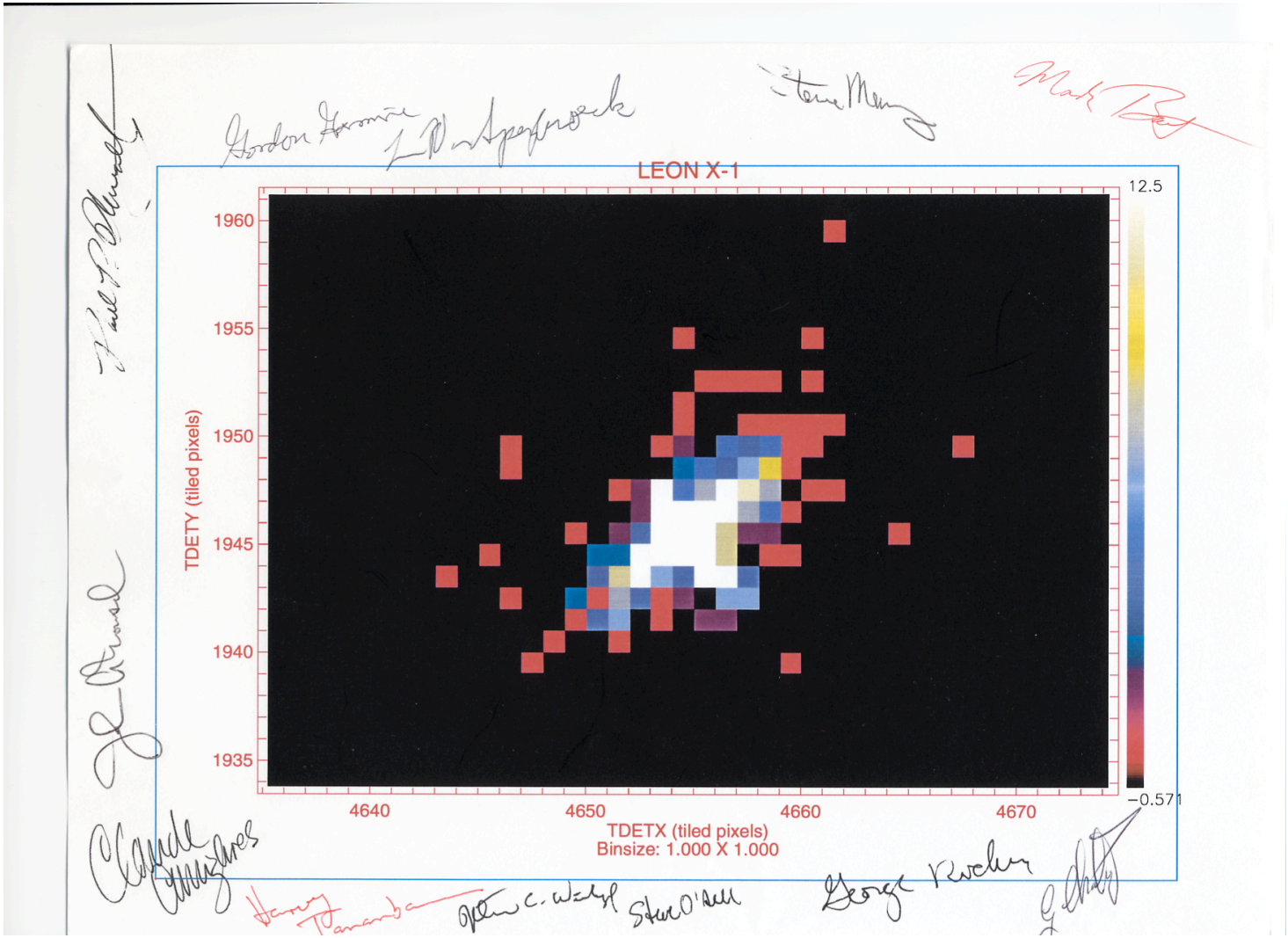

"Come on, Leon, they're great mirrors." said Weisskopf. "And, that's the first source they've ever seen, Leon X-1!" He joked.

CCD PERFORMANCE

A photoelectric interaction of an X-ray with silicon atoms in a CCD will generate electron-hole pairs. On average, the number of electrons N_e liberated by the interaction is proportional to the energy of the incident X-ray:

$N_e = E/w$, where N_e is the number of electron liberated, E is the photon energy and $w \sim 3.7 eV/e^-$ (at T = 153 K) is the mean ionization energy per electron-hole pair and is a function of the temperature of the silicon.

The variance of the charge liberated is :

$$\sigma_N^2 = F \cdot N_e = F \cdot \frac{E}{w}$$

where F, is the Fano factor and has the value $F \sim 0.135$. The effect of the statistical nature of the ionization process, the loss of charge during collection (σ_R), the noise in detector, pre-amp, main amplifier, and signal processing electronics (σ_A) , is that the primary peak produced in response to a beam of monochromatic incident photons of energy E will be approximately a Gaussian distribution with mean proportional to E and a full width at half maximum of:

$$FWHM(eV) = 2.36 \cdot 3.65 \cdot \sqrt{\sigma_N^2 + \sigma_R^2 + \sigma_A^2}$$

The strong electric field in the CCDs depletion region separates the electrons and holes before they recombine. The spectral resolution of the CCD is mainly determined by the stochastic nature of the ionization process (Fano Noise), the charge transfer properties of the CCD and the electronic noise of the readout amplifier.

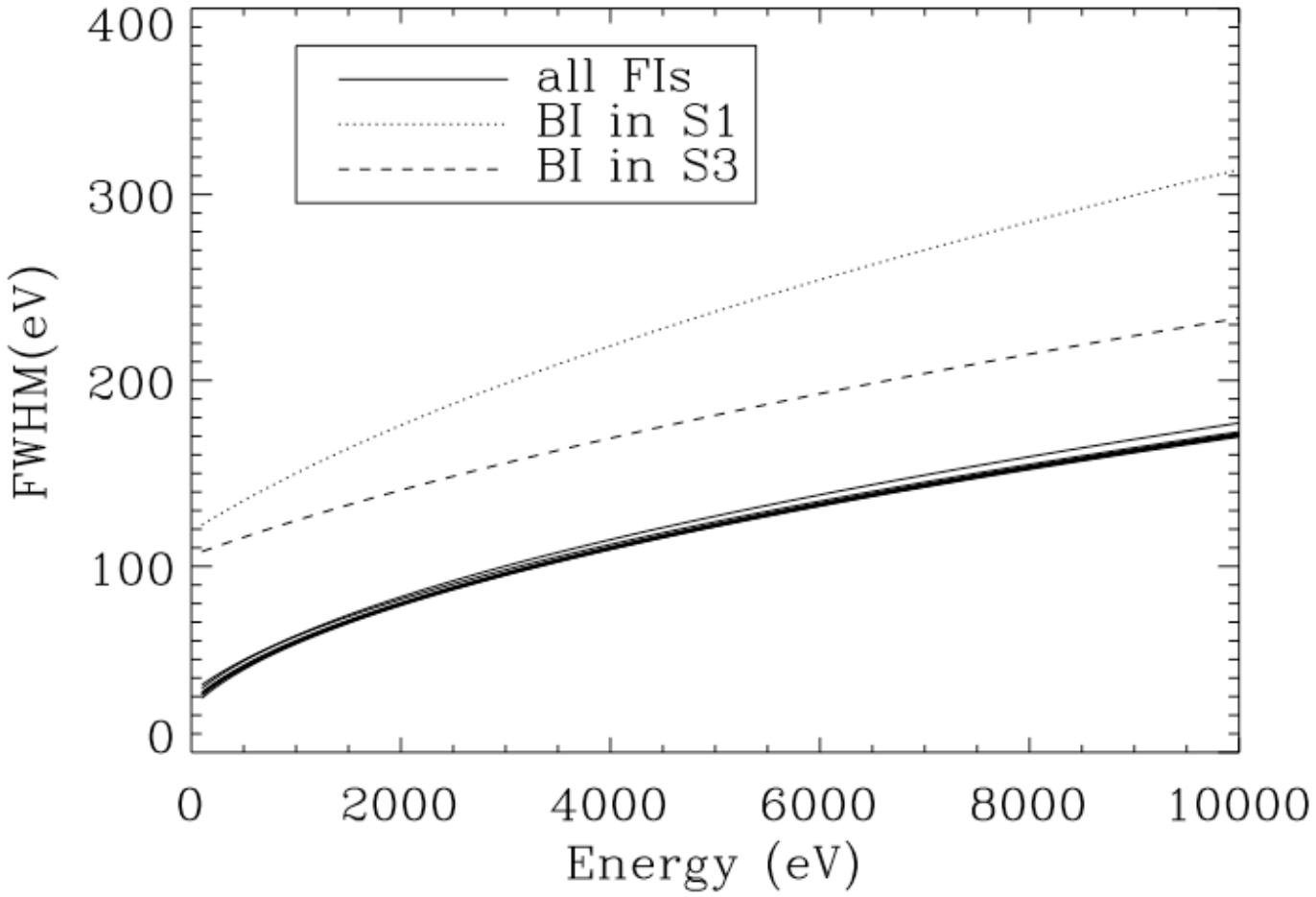

The ACIS pre-launch energy resolution as a function of energy. (Source: *CXC* Calibration group)

CCD PERFORMANCE

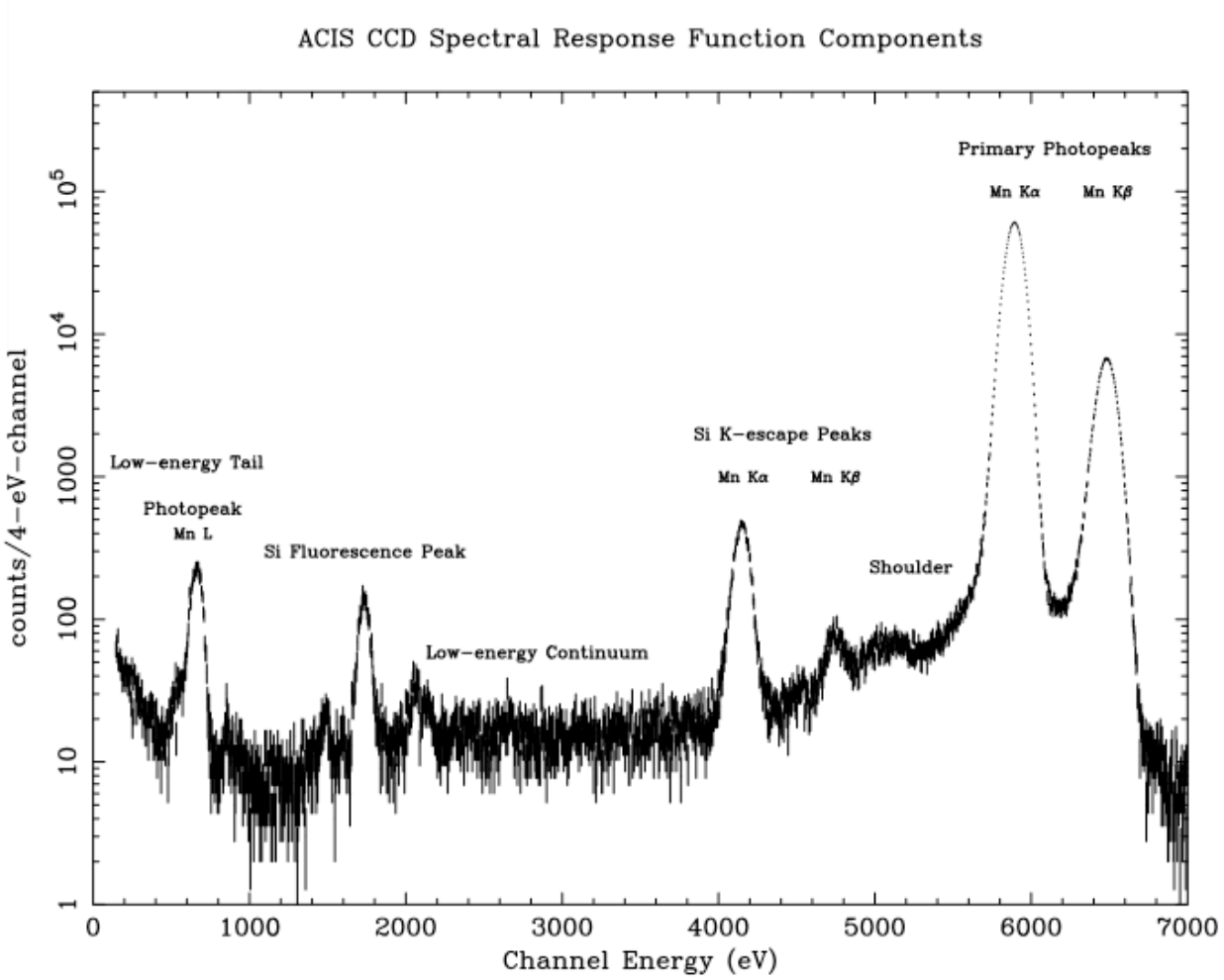

The Spectral Redistribution Function describes the probability of an instrument response in each pulse-height channel to photons of any particular energy. The ACIS spectral response shows in addition to the primary Mn peaks, the K-escape and Si fluorescence peaks, and incomplete charge collection effects by photoelectric interactions in the gates and channel stops.

CCD PERFORMANCE

Features in Spectral Response:

(a) "The shoulder" This is produced when split event threshold used in the data processing excludes valid pixels from the event amplitude summation of the 3x3 island.

(b) The low-energy continuum

(c) The low-energy tail : originates from photons interacting in the gate insulator (Prigozhin et al, 1998)

(d) Fluorescence and Escape peaks : X-rays with energies E_x greater than the Si K absorption edge of 1.839 keV can produce Si fluorescence photons of energy 1.739keV. If the fluorescent photon is detected far enough from the original interaction site it is recorded by the processing system as a separate event with an energy of E_f = 1.739keV. The escape peak is formed by the charge cloud at the original interaction site with an energy of E_x - E_f since energy of E_f has been carried away by the fluorescent photon that may escape completely from the detector or be detected separately.

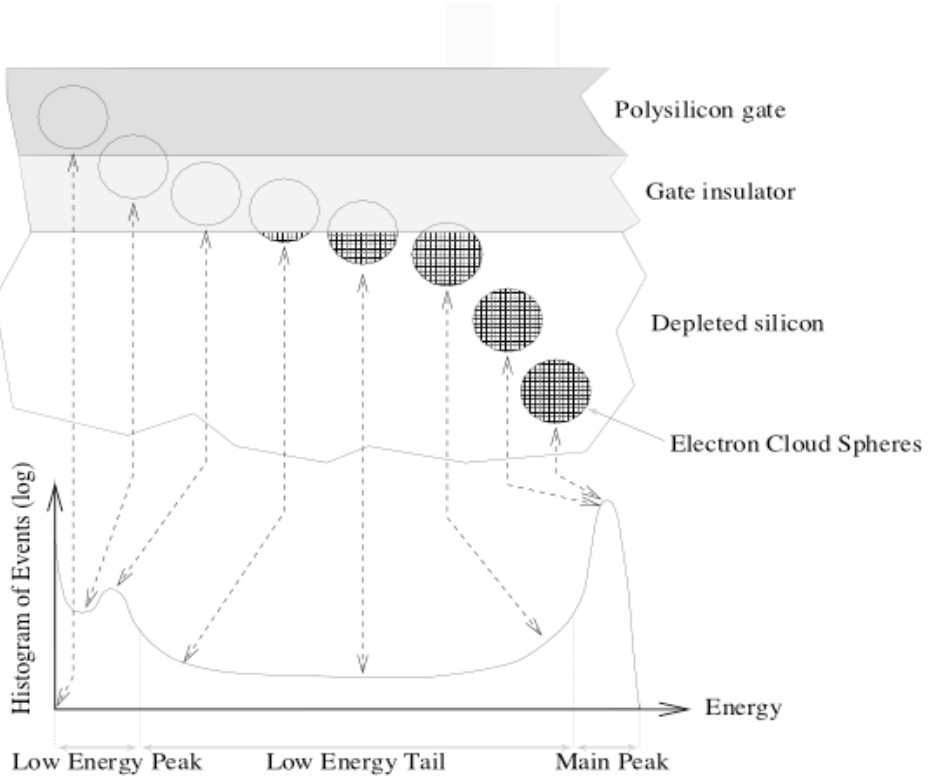

Scheme of forming low energy tail from the electron clouds generated close to $Si - SiO_2$ interface.

(Prigozhin et al., 1999, Nuclear Instruments and Methods)

CCD PERFORMANCE

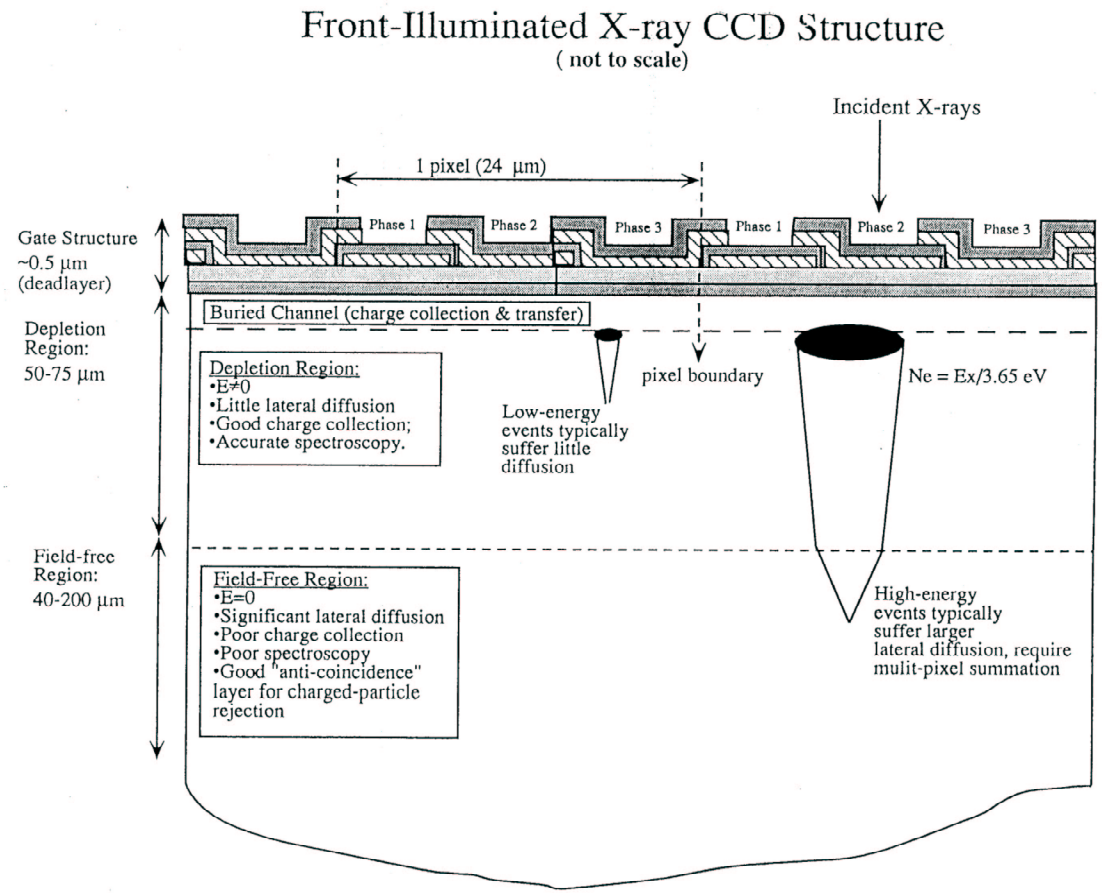

The **Quantum Efficiency** of a CCD will depend primarily on the absorbing properties of the gate structure, the insulator, the channel stops, the depths of the depletion and undepleted regions of the CCD, whether it is front or back illuminated, the absorbing properties of the optical blocking filters and the presence of any possible contaminants. Various effects that can change the effective detection efficiency of a CCD:

Pileup, CTI, event grade selection, event and split event threshold levels, deadtime due to cosmic rays

ACIS CCD Gate Structure

Parameter/Description	Typical Value (μm)
Pixel Width	24.0
Silicon Gate Thickness	0.25 - 0.30
SiO_2 Insulator Thickness	0.20 - 0.35
Si_3N_4 Insulator Thickness	0.02 - 0.04
Channel Stop Width	4.1
Channel Stop Silicon Implant Thickness	0.35
Channel Stop SiO_2 Thickness	0.45

Table 4.2: Parameters for "Slab and Stop" Model of CCD Gate Structure

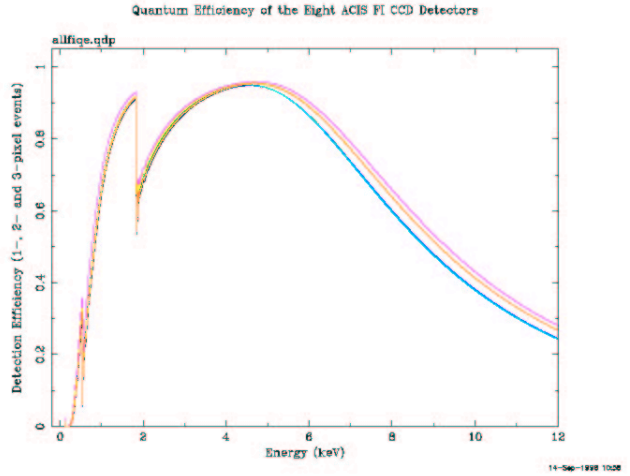

Figure 4.92: Best-fit model quantum efficiency for all ACIS FI Detectors

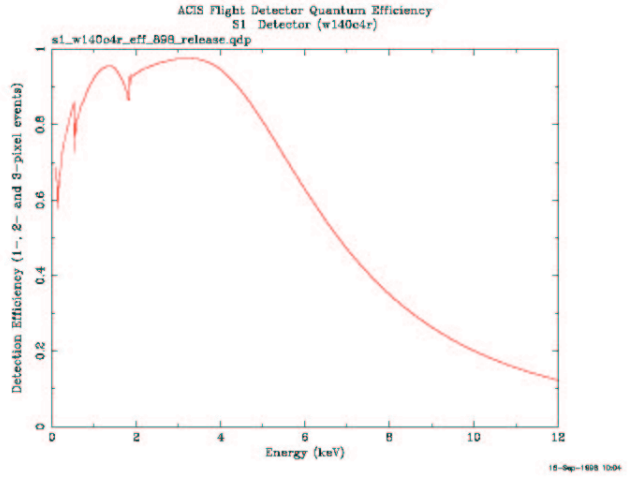

Figure 4.93: Adopted ACIS S1 (Back-illuminated) Detector Quantum Efficiency Model

CCD PERFORMANCE

Absorption Edge Structure in CCD Deadlayers

Prigozhin et al., 1998 Optical Engineering 37, 2848

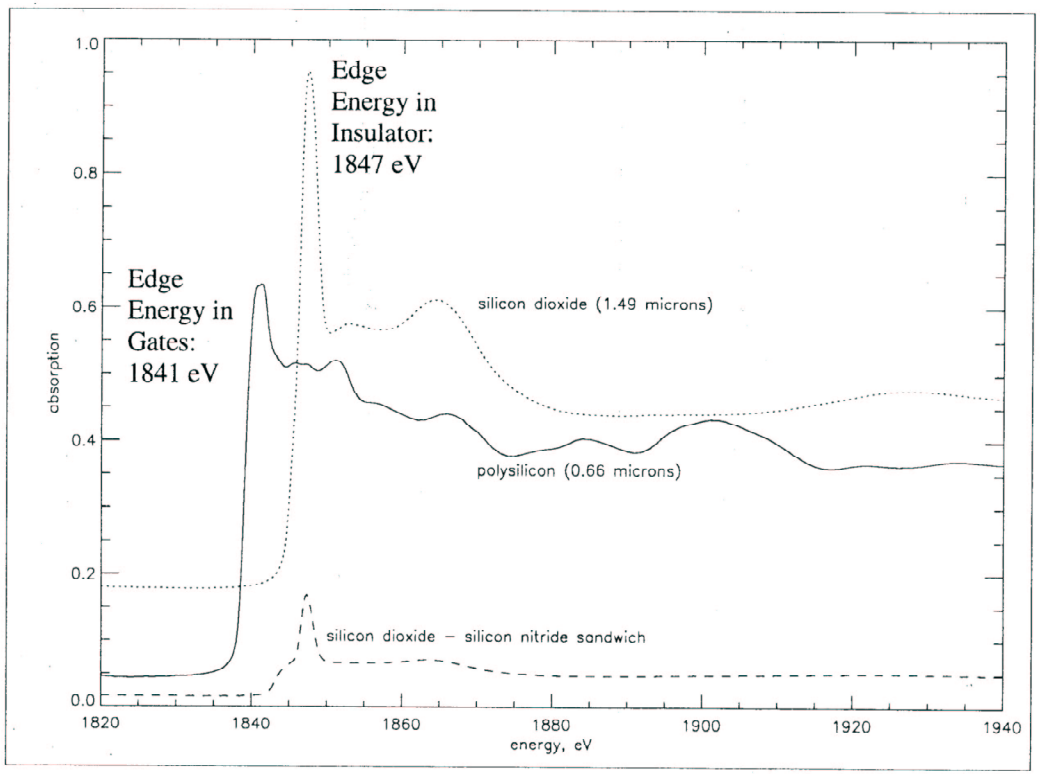

The absorption data show oscillations above the absorption edges that extend up to several hundred eV. Such structures are commonly known as extended X-ray absorption fine structure (EXAFs) and occur when atoms are in condensed matter. The oscillations arise from interference of the scattered electron wavefunction outgoing from a central atom,i, with the backscattered electron wavefunctions from nearby atoms, j.

CCD PERFORMANCE

ACIS Filters

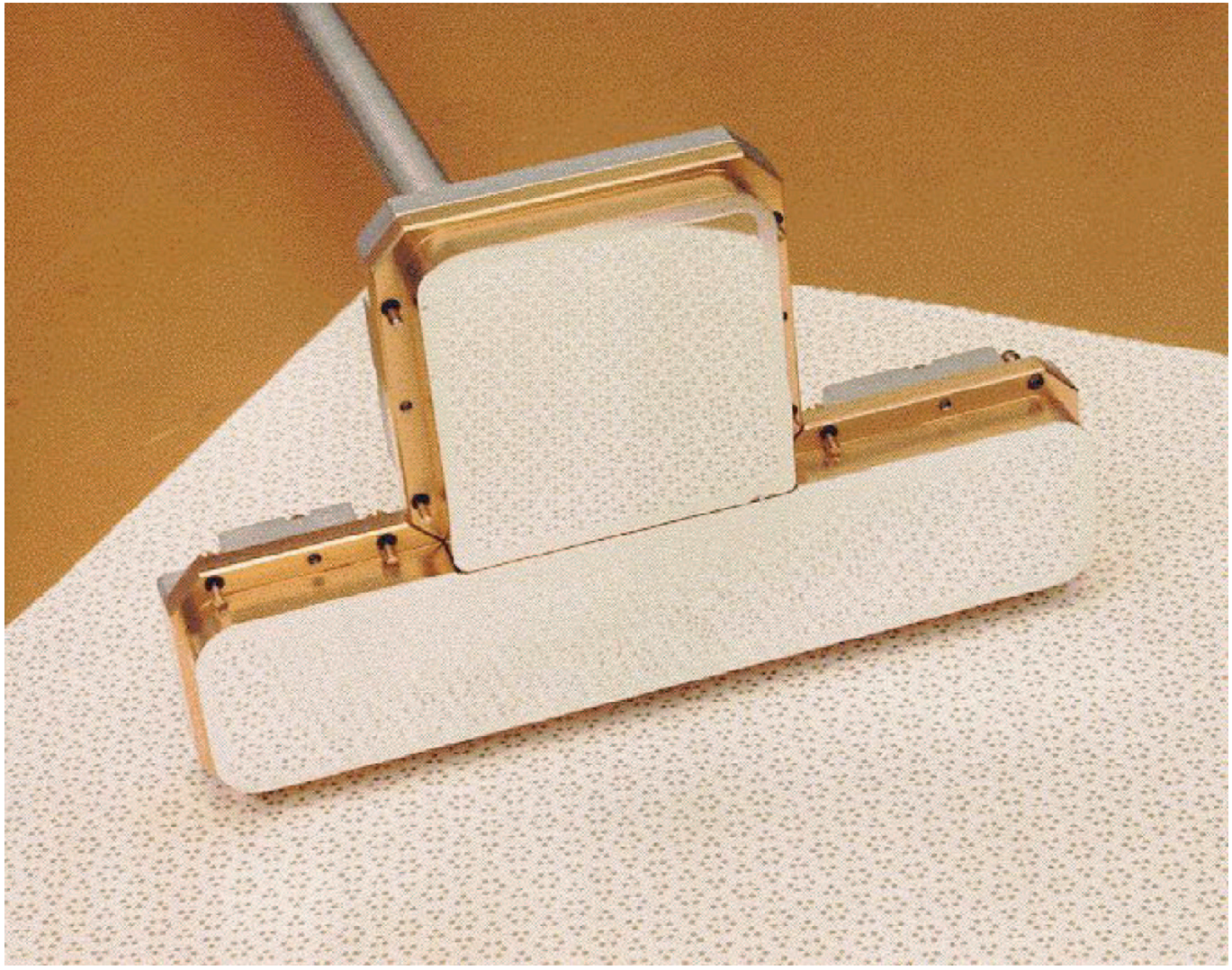

3rd INTERNATIONAL X-RAY ASTRONOMY SCHOOL

CCD PERFORMANCE

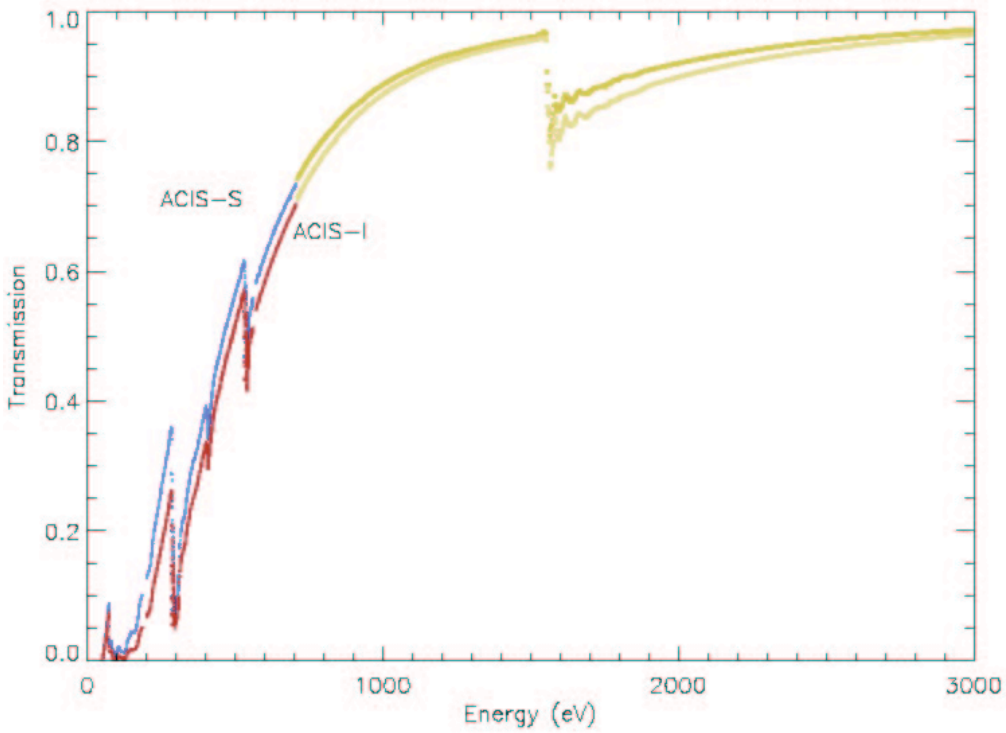

The ACIS-I and S arrays are covered by UV/Optical blocking filters (OBFs). These filters are necessary because CCD's are sensitive to UV and optical radiation. The ACIS filters consist of polyimide, $C_{22}H_{10}O_4N_2$, with a layer of aluminum coated on each side to provide optical light blocking. A method commoly used to model the X-ray transmission of filters assumes that the absorption through a multilayer filter with constituent compounds i is described by the equation : $T = \prod e^{-\mu_i \rho_i}$

Where μ_i is the mass absorption coefficient of the constituent compound i and ρ_i is the mass per unit area of the constituent compound i.

ACIS OBF Contamination

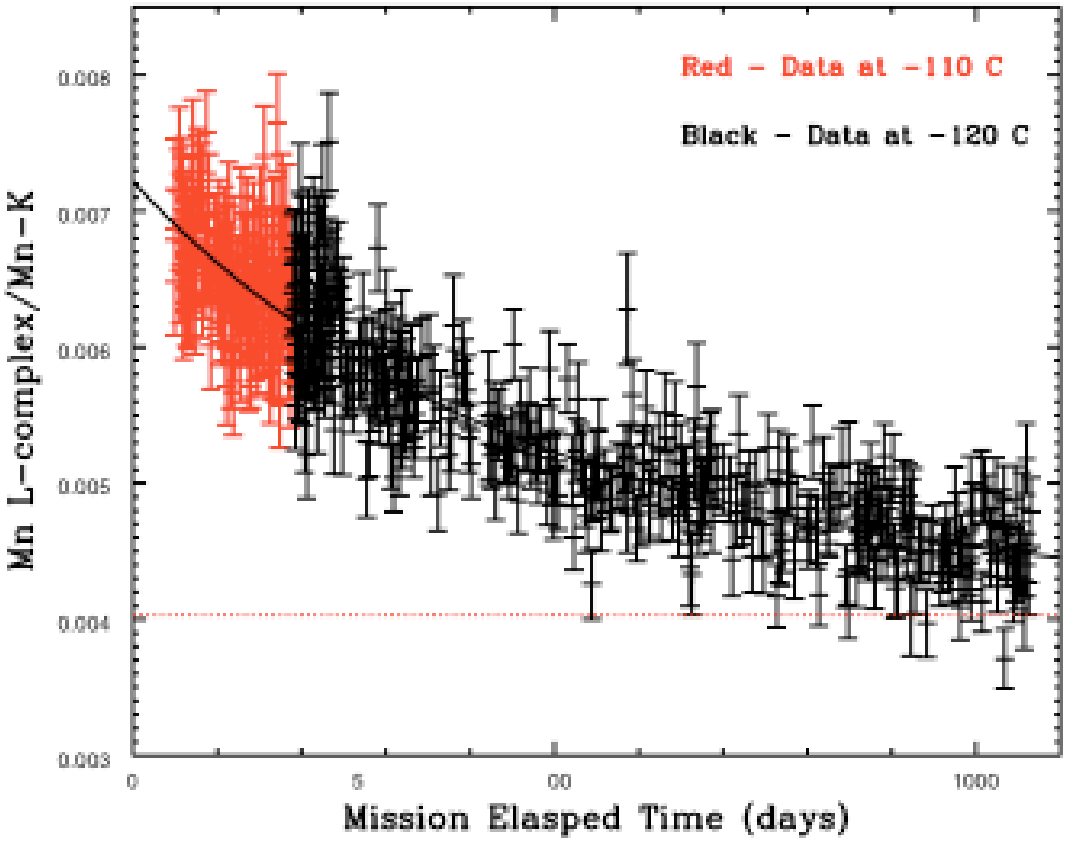

Observed decay in the ratio of the 0.67keV and 5.895keV line complexes. Measurements were performed by Catherine Grant (MIT). Plot from Plucinsky et al. 2002

ACIS OBF Contamination

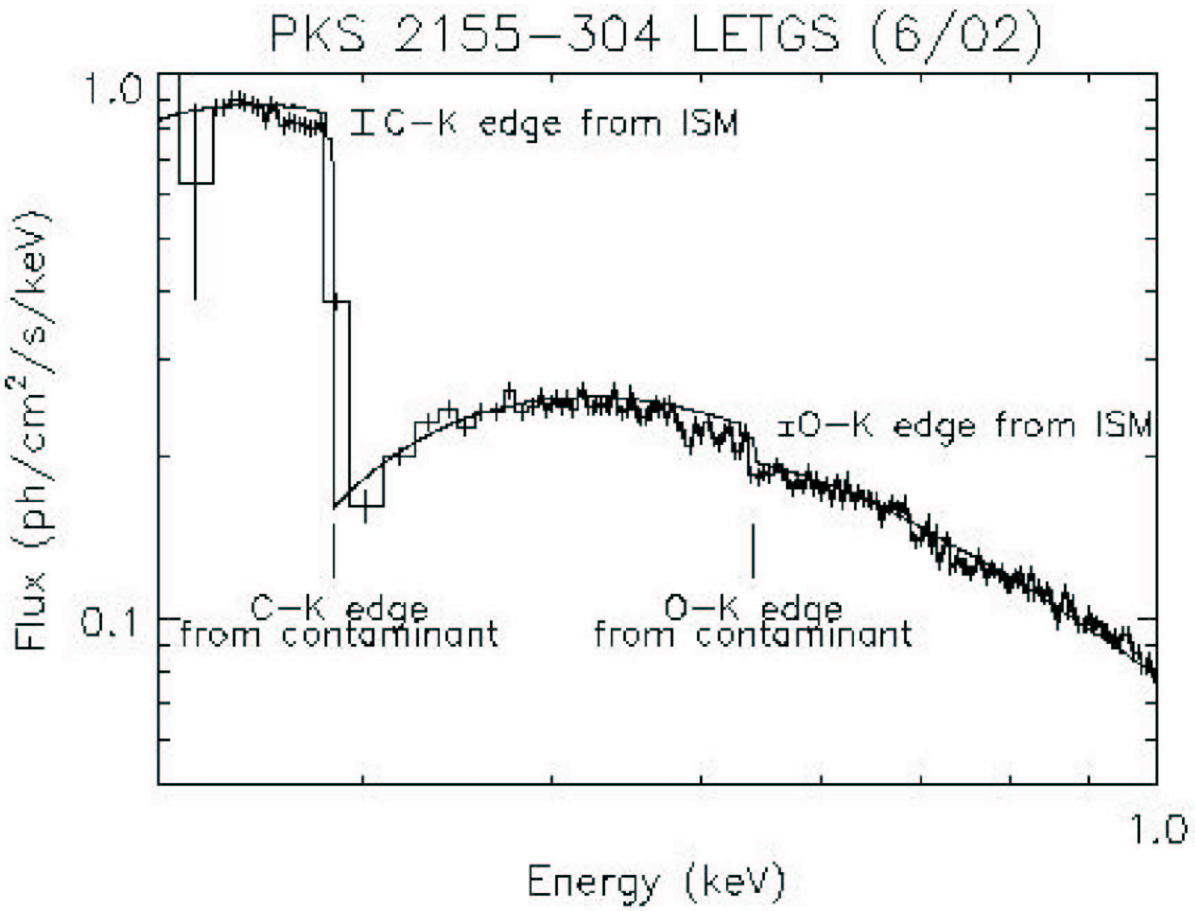

LETG/ACIS Characterization of the contamination edges, From H. Marshall (MIT)

ACIS OBF Contamination

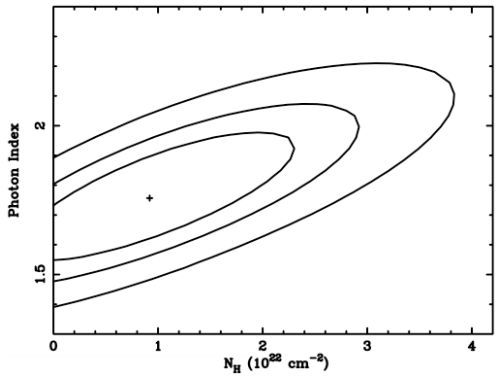

X-ray spectral results with no contamination correction

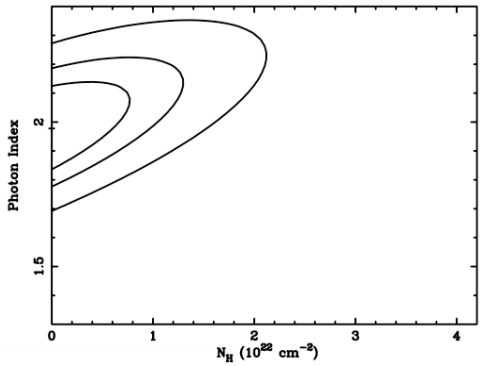

X-ray spectral results using ACISABS to modify individual ARFs.

The **ACISABS** software tool attempts at correcting for the absorption caused by molecular contamination of the ACIS optical blocking filters. The user needs to supply the number of days between Chandra launch and observation.

http://asc.harvard.edu/cont-soft/software/ACISABS.1.1.html

The composition of the contaminant was inferred from simple fits to grating observations of PKS2155 and probably will need to be updated when the composition of the contaminant is better constrained.

Applications of qe correction tools to ACIS spectra:

Properties of z>4 Quasars The data are from 9 PSS quasars at z=4.1-4.5 observed at the ACIS-S aimpoint during Chandra Cycle 3 (with typical exposure times of 4-5 ks). In total there are about 350 source counts. The X-ray spectral results shown in these figures have been obtained using C-statistic. Results provided courtesy of Christian Vignali (Vignali et al. 2002, ApJ in press)

Charge Transfer Inefficiency (CTI)

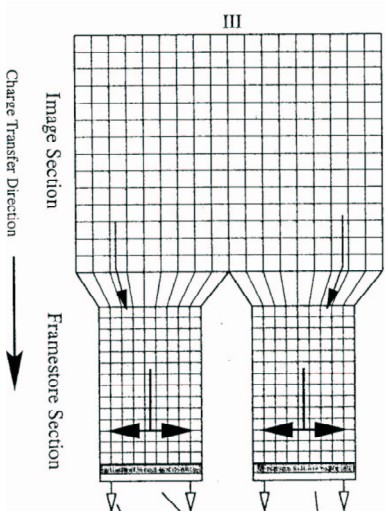

The transfer of a charge S from the furthest corner of a CCD with NxN pixels in a three phase array to its output node results in the appearance of a charge S' in the readout :

$$S' = CTE_S^{3N} x CTE_P^{3N} x S \sim CTE_S^{3N} \times S$$

CTE is the fraction of charge that makes it successfully to the next potential well after a single transfer.
The loss of charge during a transfer is mostly due to **charge traps** associated with impurities, spurious potential pockets and design faults leading to specific potential pockets at certain locations.

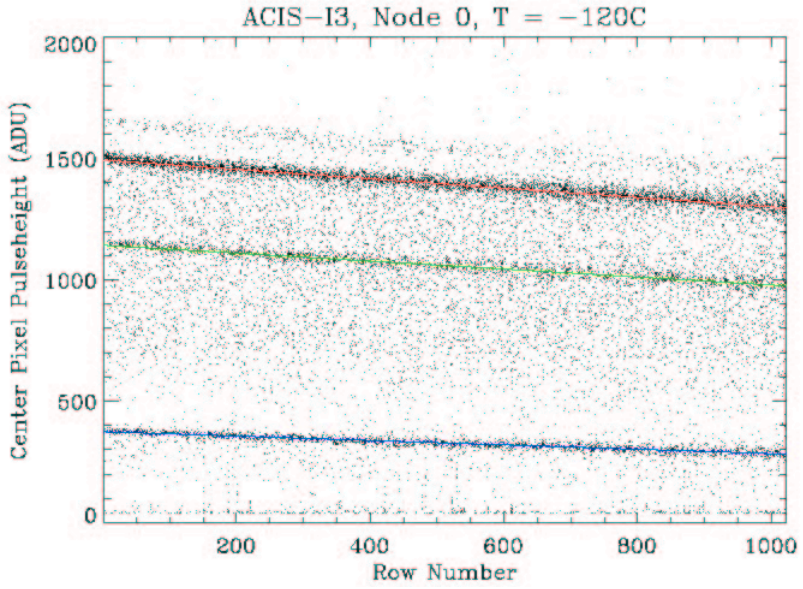

Plot of the pulseheight of an X-ray event as a function of row number when the CCD is illuminated with a monochromatic source of X-rays. Three emission lines can be clearly seen in the source spectrum : Al K, Ti K, Mn Ka. At the beginning of the mission each emission line of this plot was flat.

CTI depends, on location of charge traps, density of charge trapping sites, charge trap capture and re-emission properties.

Charge loss leads to position depended gain and spectral resolution degradation. Figure and notes from C. Grant (MIT)

Charge Transfer Inefficiency (CTI) Correction Tool

All data from the ACIS instrument on Chandra show effects from the non-zero CTI in the ACIS detectors. A corrector has been developed by L. Townsley and P. Broos (PSU) to partially remove these effects (see http://www.astro.psu.edu/users/townsley/cti/).

A detected CCD event is characterized by the total charge within the 3x3 island and the distribution of the charge (often referred to as the grade of the event) within that island.

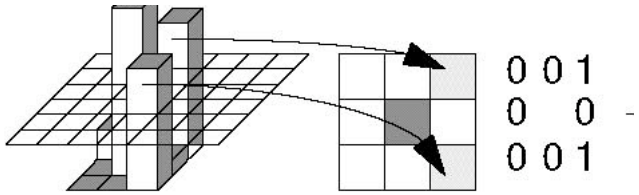

The Technique: First the calibration data are tuned to a phenomenological model of the CTI. An iterative forward-modeling technique is used to recover the best estimate of the original 3x3-pixel event island that is consistent with the CTI-corrupted event that is observed. The best estimate is returned as the CTI-corrected event.

Due to the evolution of CTI with time one may use the external calibration source to confirm the validity of the response products for a particular time period. Calibration source data are taken twice an orbit.

Photon Pileup

•Whenever the separation of two or more X-ray photons incident on a CCD is less than a few CCD pixels, and their arrival time lies within the same CCD frame readout, the CCD electronics may regard them as a single event with an amplitude given by the sum of the electron charge in the 3x3 neighborhood of the pixel with the maximum detected charge.

•Pileup may alter the grades and charges of events, thus affecting both spatial and spectral resolution. A manifestation of pile-up in observed spectra may be a reduction of detected events, spectral hardening of the continuum component and the apparent distortion of the PSF of point-like objects.

•Correcting a CCD observation of an X-ray source for pile-up is quite complicated.

Photon Pileup

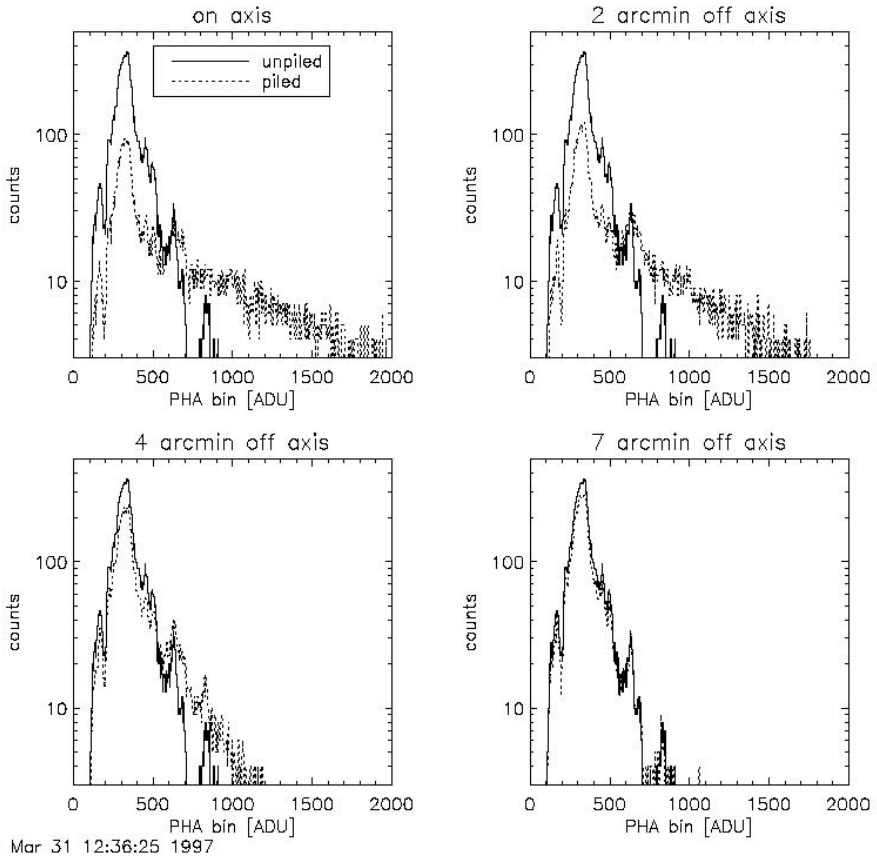

Figure 6.22: MARX simulations of the effect of pileup on the shape of the spectr true (solid line) and the detected (dotted line) spectra are shown for four differen angles. The corresponding "pileup fractions" - see Section 6.16.2 - are 46%, 4 and 2% as the image is moved progressively further off-axis. (Source: J. Kastne Wise, *CXC*)

Subpixel Resolution

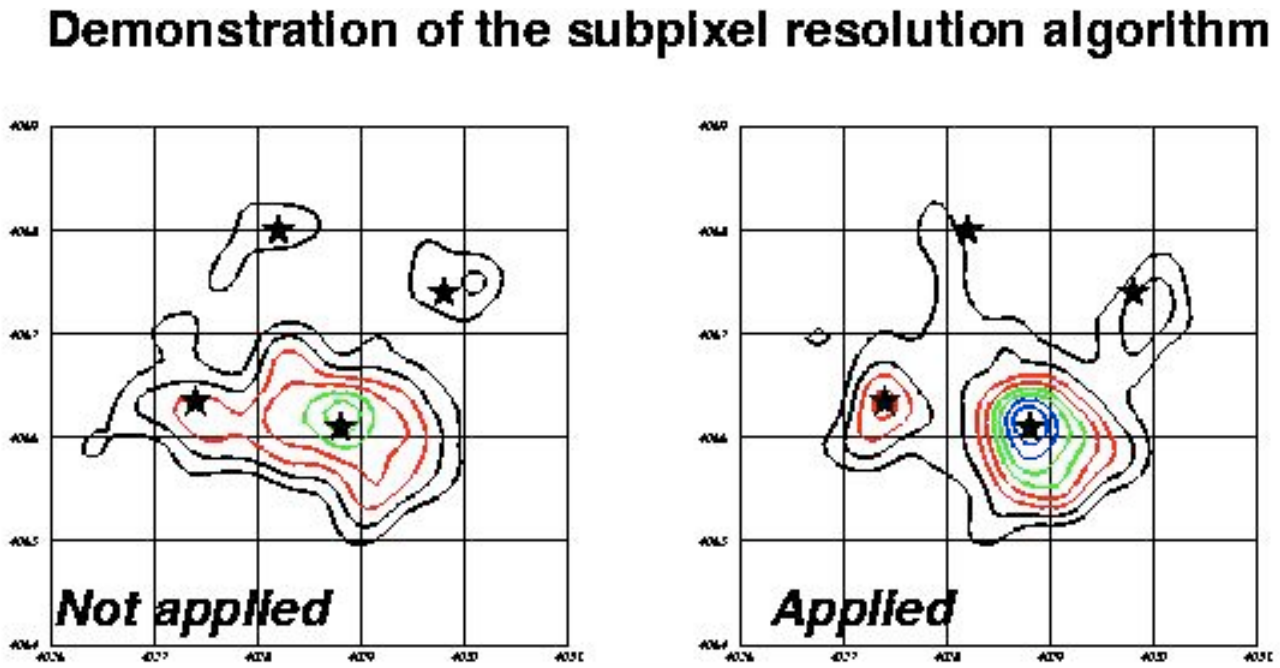

To improve the spatial resolution of Chandra, Tsunemi et al.(2001) have developed a subpixel resolution technique.The physical basis of this method is as follows; Any photon that is detected by ACIS produces a charge cloud of electrons that is collected by one or more pixels. The different arrangements of charge are referred to as ACIS grade distributions. Particular grade distributions often referred to as corner events can be used to locate the position of the incident photons to subpixel accuracy. By correcting the positions of corner pixel events the spatial resolution of ACIS is significantly improved. Figure and software available from http://www.astro.psu.edu/users/mori/chandra/subpixel_resolution.html

Spectrum of the Quiescent Background

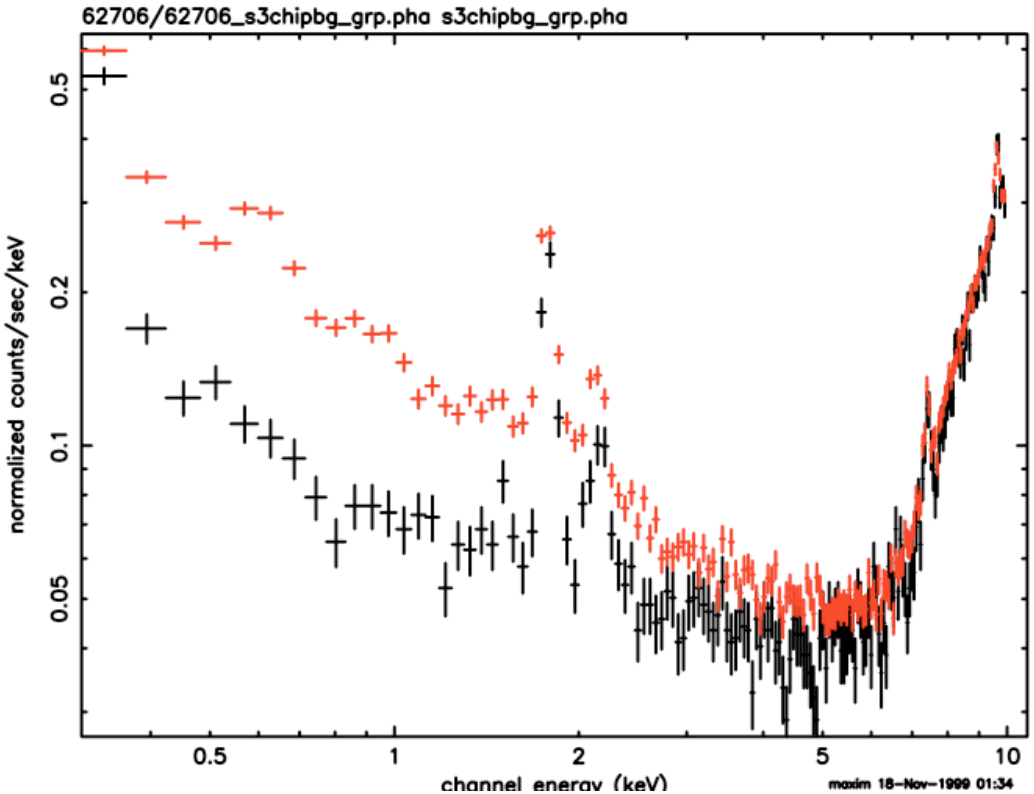

The figure illustrates contributions of the CXB and cosmic ray components to the quiescent background for chip S3 (with ACIS-S in aimpoint), after the standard grade and hot pixel cleaning and exclusion of obvious celestial sources. Black shows the data before the mirror door opening (OBSID 62706) and thus only includes the cosmic ray component, and red shows the total background (a sum of several calibration observations after the door opening). Notes and figure from M. Markevich (CfA)
http://cxc.harvard.edu/cal/Acis/Cal_prods/bkgrnd/11_18/index.html

The ACIS background consists of a relatively soft CXB contribution and cosmic ray-induced events with a hard spectrum. Most cosmic ray events can be filtered out by applying a grade filter (e.g., rejecting ASCA grades 1,5,7). After such filtering, the CXB component dominates below about 2 keV and the cosmic ray component dominates at higher energies, consistently with the pre-launch estimates.

Event Processing

Once the charge from each pixel has been read out, the onboard event processing examines each pixel and selects as events regions with bias-subtracted pixel values that exceed the event threshold and are greater than neighboring pixels. Next, valid neighboring pixels are selected as are those pixels with values greater than the split event threshold. The central pixel and the valid neighboring pixels in the 3x3 island form the grade of the event.

On-board suppression of several grades, that are thought to be produced by background, is used to limit the telemetry bandwidth.

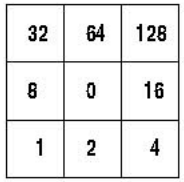

Figure 6.2: Schematic for determining the grade of an event. The grade is determined by summing the numbers for those pixels that are above their thresholds. For example, an event that caused all pixels to exceed their threshold is grade 255. A single pixel event is grade 0.

Event Processing

Standard grade set for ACIS are
ASCA grades 0,2,3,4 and 6.

Other grade selections may be useful to:

-selecting only grade 0 events may reduce pile-up and improve energy resolution with the cost of reduced S/N,

-Other grade selections have been found to reduce background

Table 6.2: ACIS and *ASCA* Grades

ACIS Grades	*ASCA* Grade	Description
0	0	Single pixel events
64 65 68 69	2	Vertical Split Up
2 34 130 162	2	Vertical Split Down
16 17 48 49	4	Horizontal Split Right
8 12 136 140	3	Horizontal Split Left
72 76 104 108	6	"L" & Quad, upper left
10 11 138 139	6	"L" & Quad, down left
18 22 50 54	6	"L" & Quad, down right
80 81 208 209	6	"L" & Quad, up right
1 4 5 32 128	1	Diagonal Split
33 36 37 129	1	
132 133 160 161	1	
164 165	1	
3 6 9 20 40	5	"L"-shaped split with corners
96 144 192 13 21	5	
35 38 44 52 53	5	
97 100 101 131	5	
134 137 141 145	5	
163 166 168 172	5	
176 177 193 196	5	
197	5	
24	7	3-pixel horizontal split
66	7	3-pixel vertical split
255	7	All pixels
All other grades	7	

Operating Modes

Timed Exposure Mode: A timed exposure refers to the mode of operation wherein a CCD collects data from a preselected amount of time - the **Frame Time**. Once this time interval has passed, the charge from the 1024x1024 active region is quickly (~41ms) transferred to the framestore region and subsequently read out through the 1024 serial registers. Notes and Figures from Chandra Proposers' Observatory Guild.

Table 6.9: CCD Frame Time (seconds) for Standard Subarrays

Subarray	ACIS-I (no. of chips)		ACIS-S (no. of chips)	
	1	6	1	6
1	3.0	3.2	3.0	3.2
1/2	1.5	1.8	1.5	1.8
1/4	0.8	1.1	0.8	1.1
1/8	0.5	0.8	0.4	0.7

Continuous Clocking Mode: The continuous clocking mode is provided to allow 3 msec timing at the expense of one dimension of spatial resolution. In this mode one obtains 1 pixel x 1024 images, each with an integration time of 3 msec.

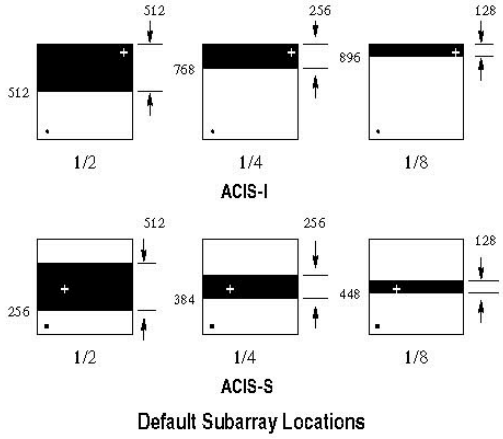

Figure 6.20: Examples of various subarrays. The heavy dot in the lower left indicates the origin

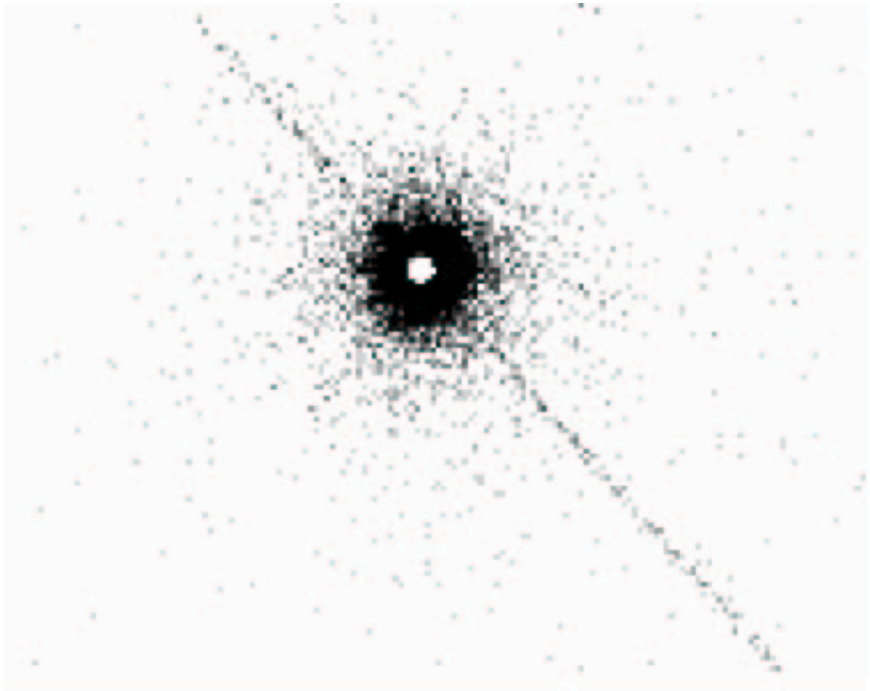

Figure 6.21: Trailed image of a strong X-ray source. The core of the image is faint due to pileup. Most events here are rejected because of bad grades. The readout direction is parallel to the trail.

Comparison Between Chandra ACIS and XMM-Newton-EPIC

Characteristics of Some "Current Generation" X-ray CCDs

Characteristic	Chandra-ACIS		XMM-Newton-EPIC	
	FI	BI	MOS	PN
Electrode Technology	3-poly MOS	3-poly MOS	3-poly MOS (open electrode)	Junction
Illumination	Front	Back	Front	Back
Pixel Size (μm)	24	24	40	150
Format	1k x 1k	1k x 1k	600 x 600	200 x 64
Detectors in Focal Plane	8	2	2 x 7	12
Focal Plane Sensitive Area (cm^2)	48 + 12		2 x 40	35
System Noise (e^-, RMS)	2	3	5	5
Single Channel Readout Rate (kpix s^{-1})	100	100	128	43
Readout Channels per Detector	4	4	1	64 analog + 1 A/D
Full Focal Plane Frame Time (s)	3.2	3.2	2.8	0.074
Charge Transfer Inefficiency	$< 3 \times 10^{-6}$	$< 1 - 3 \times 10^{-5}$	$< 3 \times 10^{-6}$	$\sim 10^{-4}$
Depletion Depth (μm)	75	40	40	300
Energy Resolution (eV, FWHM):				
at 0.525 keV	45	100	>80	70
at 5.9 keV	135	150	135	135
CCD Manufacturer	MIT/Lincoln	MIT/Lincoln	MAT (EEV)	MPE/HLL

CCDs in Future X-ray Astronomy Missions

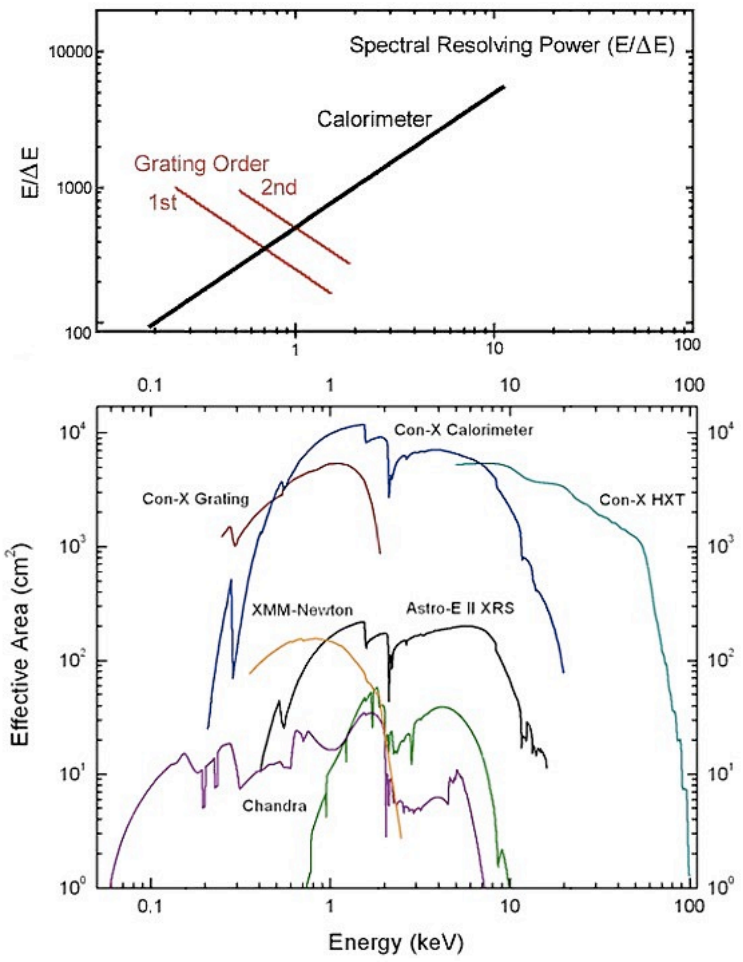

CCDs are presently used onboard *Chandra* and *XMM-Newton*. These two major observatories are expected to continue to provide images and spectra of the X-ray Universe into the near future (5-10 years). A smaller mission HETE -2 also makes use of CCDs to study gamma ray bursts.

Future missions that plan to include CCDs are *Swift* scheduled to launch by the end of 2003, *ASTRO-E2* scheduled to launch in early 2005, and *Constellation-X* scheduled to launch around 2013.

ASTRO-E2 and *Constellation-X* will both have X-ray calorimeter detectors which have energy resolution of order several eV.
The thermal and light rejection requirements for calorimeters makes it necessary to use thick filters which reduce the response of these devices significantly below 1 keV. In addition, at energies below 1keV grating spectrographs combined with CCDs provide better energy resolution as seen in the figure.